MR Physics-Based Snake Tracking and Dense Deformations from Tagged Cardiac Images

Amir A. Amini, Rupert W. Curwen, R. Todd Constable, and John C. Gore

Departments of Diagnostic Radiology, Electrical Engineering,
and Applied Physics
Yale University
New Haven, CT 06510

Abstract

MRI is unique in its ability to non-invasively and selectively alter tissue magnetization, and create grid patterns on a soft, deforming body such as the heart muscle. We track motion of myocardial tag lines with energy-minimizing B-spline snakes. Oriented tag templates are first constructed by simulating the MR imaging process. The templates are subsequently correlated with the image data, giving rise to an energy landscape, which is optimized over with dynamic programming. Tracking the valleys of the energy landscape with snakes allows for measurement of MR tag deformations due to tissue motion. Tissue deformation parameters corresponding to strain, vorticity, and compression/expansion of myocardial regions are also derived. The latter two quantities are computed from a modified thin-plate spline reconstruction of a dense motion field.

1 Introduction

Non-invasive techniques for assessing the dynamic behavior of the human heart can be invaluable in the diagnosis of heart disease, as abnormalities in the myocardial motion sensitively reflect deficits in blood perfusion. In this paper, we discuss our approach to measurement of motion from tagged MR images.

Leon Axel developed the SPAMM technique in which a grid of intersecting planes of altered magnetization is placed within the myocardial tissue [2]. During heart contractions, the grid patterns move, allowing for visual tracking of the grid intersections over time. In this paper, we describe techniques suitable for measuring mechanical strain from SPAMM tagged MR images, methods for reconstructing a dense motion field from these images, and new indices of myocardial deformation from the reconstructed motion fields.

An alternate tagging method described by Zerhouni and co-workers applies a radial array of thin striped tags over a short axis view of the heart [8]. Again, with star-burst tags, motion of the tissue leads to deformation of the pattern, and allows for visual tracking of the tag line over time. In this paper, we describe a new B-spline snake algorithm for tracking star-burst tagged images. In constructing the energy field for spline optimization physics of MR imaging is utilized.

2 NMR Tagging

In a normal MR image, the image intensity is obtained by measuring the NMR signal corresponding to each tissue location. In the presence of an external magnetic field, the local nuclear spins sum to provide the tissue magnetization. Application of an RF pulse of a specific power and frequency content leads to absorption of energy by the spin system, and the magnetization is rotated by 90 degrees, into the transverse plane, where it precesses and induces a signal in a coil around the sample. In the process of returning to the original orientation (this process is known as relaxation), a coil measures the local generated signal for spin-echo images. The detected signal is a function of tissue relaxation parameters, as well as the local proton density, and may be described analytically as:

$$f_1(x,y) = AM_0(x,y)e^{-\frac{T_E}{T_2(x,y)}} \left[1 - e^{-\frac{T_R}{T_1(x,y)}}\right] \quad (1)$$

where A is the system gain, and M_0 is the equilibrium magnetization. T_1 and T_2 are the tissue relaxation parameters, and T_E and T_R are imaging parameters.

In a tagged MR image, a series of selective RF pulses are applied prior to the conventional imaging protocol decribed above, rotating the tissue magnetization. The aggregate effect of the pulse sequences gives the following expression for the tag intensity:

$$f_2(x,y) = (1 - cos(\phi(x)))e^{-T_R/T_1} + (cos(\phi(x)) - 1)e^{-T_D/T_1} \quad (2)$$

In (2) , ϕ is the flip-angle, and T_D is the time between application of the tag and the imaging pulse sequence. As in Guttman [6], we simulate the Bloch equations for the MR imaging process, and obtain a sequence of tag profiles as a function of time. The tag profiles approximate inverted Gaussian functions which undergo T_1 tissue relaxation, becoming less visible in later phases of the heart cycle (fig. 1). In these simulations the following parameters were used: duration of tag pulse was $T_s = 1.8$ msec, Gyromagnetic Ratio was 26800 HZ/G, gradient strength was $G_x = 0.052$ G/mm, $T_R = 1$ sec, and $T_1 = 0.5$ sec. The RF pulse had the following form:

$$B_1(t) = V_0 v(t) w(t) cos 2\pi f_0 t \hat{x} \quad (3)$$

where v is a sinc pulse, w is the Hamming window, and $V_0 = 0.09$ G.

3 Energy Field

The simulation returns a predicted tag profile in the direction perpendicular to image tag lines as a function of time and is normalized to lie between zero and one. To create an energy field, the following approach is taken. For points within tag lines in the the vertical orientation, a set of profiles are concatenated along the vertical axis to create a correlation kernel, g_1. The correlation kernel is then successively rotated to create kernels along other orientations. Additional energy fields are constructed using correlation kernels for tag endpoints. Let the image be represented by g_2. The normalized correlation, $\rho(x, y)$ is

$$\frac{\int\int g_1(x+\delta_x, y+\delta_y) g_2(x,y) dxdy}{\left\{\int\int g_1^2(x+\delta_x, y+\delta_y) dxdy \int\int g_2^2(x,y) dxdy\right\}^{1/2}} \quad (4)$$

with $0 \leq \rho \leq 1$, and with $\rho = 1$ when g_1 is a constant multiple of g_2. In order to increase the discrimination power of the technique the energy field is set to $-\rho^n(x, y)$, where n is a positive integer less than 10. Endpoint energy fields are termed ρ_e, and are obtained from correlating endpoint masks with the tag data. For each tag endpoint, a correlation mask is generated, and is used to construct endpoint energy images for subsequent frames. These kernels essentially have half of the window filled with tag profiles, and depending on the tag line, have half filled with zero intensities, or intensities from surrounding organs. Currently, tag endpoint coordinates are specified in the first frame. All subsequent endpoints are determined by the algorithm.

4 B-Spline Snakes with DP

We use B-spline snakes [7, 3] to represent image tag lines. The spline is given by the following expression:

$$\alpha(u) = \mathbf{u}^T \mathbf{M} \mathbf{P} \quad (5)$$

where $\mathbf{u}$ is a column vector of powers of u, the spline parameter, $\mathbf{P}$ is a sequence of control points, and $\mathbf{M}$ is a matrix which blends the control points. The approach is to minimize the following expression along tags:

$$E_{total} = -\{\int \rho^n(\alpha(u))du + \rho_e^n(\alpha(0)) + \rho_e^n(\alpha(u_{max}))\} \quad (6)$$

In equation (6), the first term maximizes ρ^n along the length of the snake, and second and third terms attract the snake to the endpoint of tag lines.

The discrete form of E_{total}, for a quadric spline may be written as:

$$E_{total} = E_0(p_0, p_1, p_2) + \cdots + E_{N-3}(p_{N-3}, p_{N-2}, p_{N-1})$$

where p_i are the B-spline control points. Dynamic Programming (DP) [1] may be used to optimize the curve in the control point space to minimize E_{total} using the following recurrence

$$S_i(p_i, p_{i+1}) = \min_{p_{i-1}} E_{i-1}(p_{i-1}, p_i, p_{i+1}) + S_{i-1}(p_{i-1}, p_i) \quad (7)$$

for $i \geq 2$, and $S_1(p_1, p_2) = \min_{p_0} E_0(p_0, p_1, p_2)$. In general, for an order k B-spline, S_i is a function of k control points. Also, note that the minimization yields the optimal open spline, as is the case for a tag line. In order to find a closed snake, one performs M applications of the above recurrence, where M is the number of possible choices for the endpoint p_i, and for each optimization fixing the *end point* to be one of the M choices, repeating for all M possibilities, and finally choosing the minimum. Figure 2 shows the initial star-burst image and results from the DP algorithm. Figure 3 shows the energy field for a diagonal tag line, and for one endpoint of the same tag line.

5 Dense Velocity Field Estimation and Tissue Deformation Indices

In the case of SPAMM grids, from following grid line intersections, we obtain displacement information at a set of loci in the image. In the case of star-burst images, tracking the tag lines will yield displacement information at points where the tag lines intersect the heart wall. Clearly, it is desirable to obtain a dense field of displacement vectors so that myocardial motion can be inspected at all points falling within the myocardium.

As with the case of tag lines, we perform spline approximation of the data [5, 4] for providing dense motion information. Two variational principles are posed which we numerically solve, yielding components of the displacement vector field for all pixels in the LV myocardium[1]:

$$\sum_{(i,j)\in D} (d - d_{ij})^2 + \lambda \int\int d_{xx}^2 + d_{yy}^2 + 2d_{xy}^2 dxdy \quad (8)$$

In the above expression, d is used to denote the u, or v component of displacement, λ is in general a non-negative function of x and y and controls the degree of smoothing, and D is the set of points with known displacement information. Successive Over Relaxation (SOR) is used to solve the resulting discrete linear systems of equations to obtain dense displacement information. This method calculates LV displacement at all points of a 2D tagged cardiac MR image utilizing the tracked image tag information. Results of dense motion estimation from 2 consecutive frames of a SPAMM tagged MR image sequence are shown in figure 4.

5.1 Measures for Tissue Expansion, Contraction, and Circulation

In previous work, authors have reported measuring such quantities as torsion, and rotational motion of the tissue. However, with previous techniques, this information could only be obtained at a specific set of points within the myocardium. With the methods described, we can obtain displacement vectors on all parts of the

[1] We would like to perform the spline approximation without knowledge of LV boundary. One idea which is currently being pursued is to normalize the derivative component of the integrand with respect to components of the image gradient of an untagged MR cardiac scan performed at the same time point of the ECG wave.

myocardium. From this information, we obtain *differential* vector quantities which describe local rotations and expansions.

Tissue Expansion and Contraction

Expansion or contraction of the myocardium in an arbitrary area within the LV wall between the endocardial and epicardial surfaces may be written as:

$$\int_{\Gamma} \vec{V} \cdot \vec{n} ds = \int_{A} \nabla \cdot \vec{V} dA \tag{9}$$

where the integral on the left is a line integral computed on a curve Γ which bounds the myocardial mass of interest, $\vec{n}$ is the normal to Γ, and $\vec{V}$ is a dense displacement vector field. The integral on the right is over the area bounded by Γ, and $\nabla \cdot \vec{V}$ is the divergence of the vector field. This provides an easy way to compute a quantitative measure of tissue expansion. The strength of this measure is that it is invariant to rigid body motion, and so can be used as a measure of compressibility, of non-rigid deformation, or of tissue expansion, or contraction.

Circulation

Torsion has been described to be of major significance in the study of LV. We can evaluate circulation accurately around any contour bounding the LV myocardium:

$$\oint_{\Gamma} \vec{V} \cdot \vec{t} ds = \int_{A} (\nabla \times \vec{V})_n dA \tag{10}$$

where Γ is a planar contour, t is the tangent to such a curve, n is the binormal of the curve, and the integral is evaluated around Γ. $(\nabla \times \vec{V})_n$ is the component of curl of $\vec{V}$ perpendicular to the plane of Γ describing *infinitesimal* circulation of the displacement vector field at a point. It is important to note that this information can be evaluated around any planar contour which passes through the myocardium.

5.2 Strain

Strain is a measure of local deformation of a line element due to tissue motion and is independent of the rigid motion of the LV. To compute the local 2D strain for a given triangle, correspondence of the 3 vertices with a later time is sufficient [2]. With such information known, an affine map F is completely determined. By the *polar decomposition theorem*, F can be decomposed as $F = R \cdot U$, where R is a rotation matrix, and U is a symmetric matrix representing the 2D strain. Under the linear motion assumption, strain in the direction of a vector $\vec{x}$ can be expressed as

$$\Sigma = \frac{1}{2}\left(\frac{|Ux|^2}{x^T x} - 1\right) \tag{11}$$

Two directions within each such triangle are of particular interest, namely, the directions of principal strain, representing the maximum and minimum stretch within a triangle, and corresponding to the eigenvectors of U. The results of strain analysis done on images of figure 5 is shown in figure 6 where the maximum and minimum principal strain directions and values are shown. It should be pointed out that extension of quantities obtained from equations (8), (9), (10), and (11) to 3D is possible with tagging. Naturally, there are three principal strain directions in 3D.

6 Conclusions

In conclusion, we have described new computer vision algorithms, which utilize the physics of medical imaging for tracking with energy-minimizing snakes. From a clinical standpoint, the computer vision reconstruction algorithm described here may be useful as an initial step in measurement of local myocardial deformation. Mechanical strain can also be measured with suitable accuracy from tagged images.

References

[1] A. A. Amini, T. E. Weymouth, and R. C. Jain. Using dynamic programming for solving variational problems in vision. *IEEE Transactions on Pattern Analysis and Machine Intelligence*, 12(9):855–867, 1990.

[2] L. Axel, R. Goncalves, and D. Bloomgarden. Regional heart wall motion: Two-dimensional analysis and functional imaging with mr imaging. *Radiology*, 183:745–750, 1992.

[3] A. Blake, R. Curwen, and A. Zisserman. A framework for spatio-temporal control in the tracking of visual contours. *International Journal of Computer Vision*, 11(2):127–145, 1993.

[4] F. Bookstein. Principal warps: Thin-plate splines and the decomposition of deformations. *IEEE Transactions on Pattern Analysis and Machine Intelligence*, 11(6):567–585, 1989.

[5] W. Grimson. An implementation of a computational theory of visual surface interpolation. *Computer Vision, Graphics, and Image Processing*, 22:39–69, 1983.

[6] M. Guttman, J. Prince, and E. McVeigh. Tag and contour detection in tagged mr images of the left ventricle. In *IEEE Transactions on Medical Imaging*, in press.

[7] S. Menet, P. Saint-Marc, and G. Medioni. B-snakes: Implementation and application to stereo. In *Proceedings of Third International Conference on Computer Vision*, pages 720–726, 1990.

[8] E. Zerhouni, D. Parish, W. Rogers, A. Yang. and E. Shapiro. Human heart: Tagging with mr imaging – a method for noninvasive assessment of myocardial motion. *Radiology*, 169:59–63, 1988.

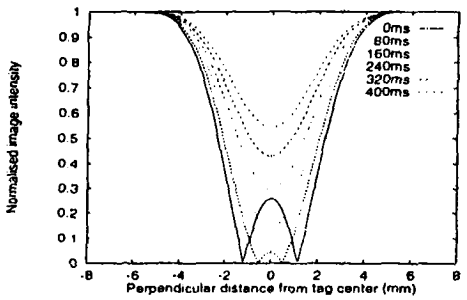

Figure 1: Simulated tag profiles for successive time instants.

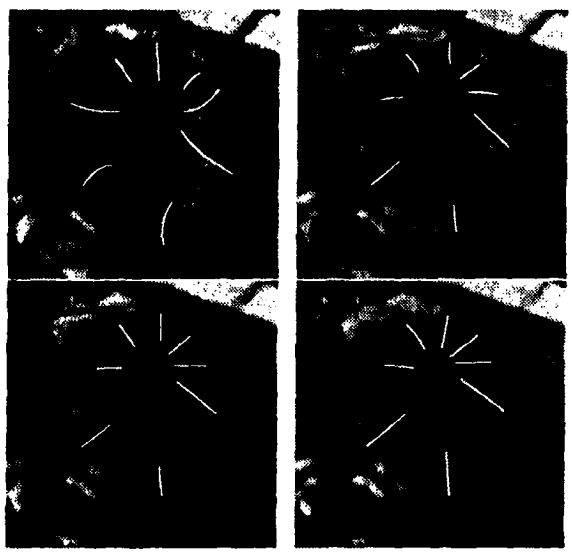

Figure 2: Results from tracking with DP snakes. The initial, unoptimized placement of B-Spline snakes is shown in top left. Tag lines in subsequent frames are localized and tracked automatically.

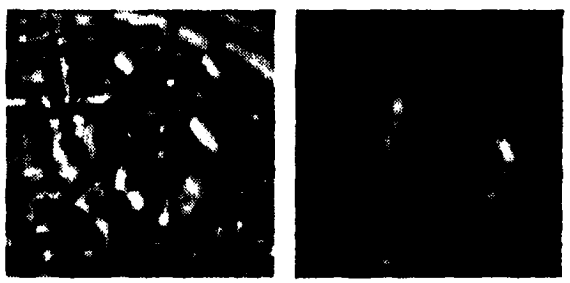

Figure 3: Energy field for frame 1 in the previous figure. ρ^n and ρ_e^n are displayed for a diagonal tag line, and one endpoint.

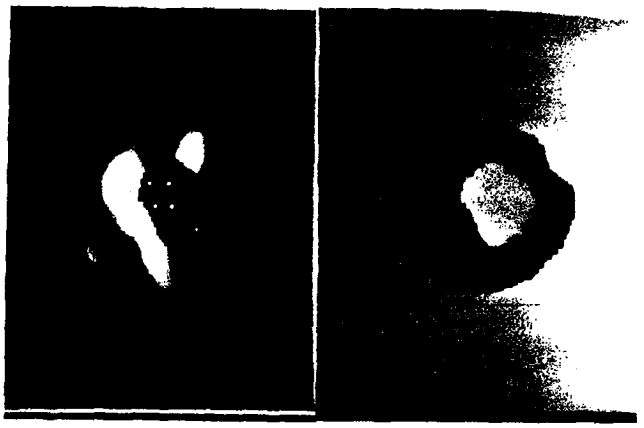

Figure 4: Reconstruction of dense u and v components of displacement from 2 frames of a SPAMM tagged image.

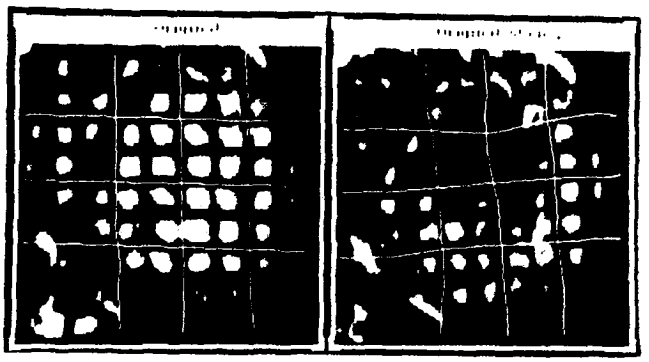

Figure 5: Two consecutive frames of SPAMM tagged cardiac images. Hand-traced tag lines are superimposed.

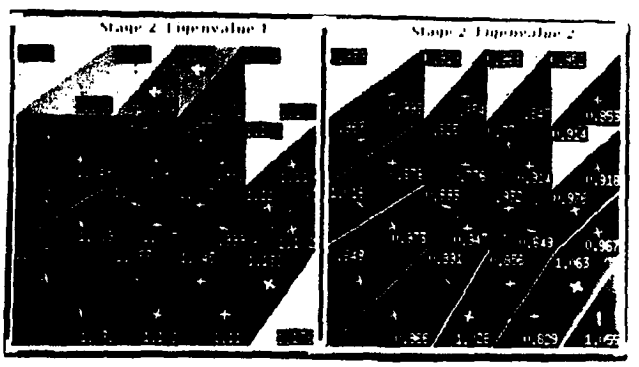

Figure 6: Strain measurement made from figure 5: principal strain values and directions.